

Supplementary Information for Low-Frequency Vibrational Spectroscopy: A Powerful Tool for Revealing Crystalline Magnetic Structures in Iron Phosphate Crystals

Zihui Song,[†] Xudong Liu,[‡] Anish Ochani,[¶] Suling Shen,[‡] Qiqi Li,[‡] Yiwen Sun,[‡]
and Michael T. Ruggiero^{*,†,§}

[†]*Materials Science Program, University of Vermont, Burlington, VT 05405 USA*

[‡]*Department of Biomedical Engineering, Shenzhen University, No. 3688, Nanhai Road,
Nanshan District, Shenzhen, Guangdong, China*

[¶]*Department of Chemistry, SUNY College at Old Westbury, Old Westbury, NY 11568,
USA*

[§]*Department of Chemistry, 82 University Place, University of Vermont, Burlington, VT,
05405 USA*

E-mail: Michael.Ruggiero@uvm.edu

1 Methods

1.1 Experimental

1.1.1 Preparation of Anhydrous FePO_4

FePO_4 was prepared according to the previously published procedure.¹⁻³ Iron(III) phosphate hydrate ($\text{FePO}_4 \cdot x\text{H}_2\text{O}$, Alfa Aesar), without any further purification, was dehydrated in an oven for 6 hrs at 600°C.⁴ The dehydrated product was confirmed to be the α -quartz type iron (III) phosphate (FePO_4) by PXRD.

1.1.2 Powder X-ray Diffraction

All experimental PXRD patterns were acquired using a Bruker Advanced powder diffractometer using Cu K_α radiation ($\lambda = 1.5418 \text{ \AA}$), and were collected at room temperature. Diffraction patterns were obtained at 2θ values from 5 to 50°.

1.1.3 Terahertz Time-Domain Spectroscopy

All THz-TDS data were collected using a commercial Teraflash Pro spectrometer platform (Toptica Photonics AG, Munich, Germany). A pair of fiber-coupled InGaAs photoconductive terahertz antenna (PCA) were used as emitter and receiver, and two pairs of off-axis parabolic mirrors were used to collimate and focus the terahertz radiation, respectively. The entire spectrometer was enclosed and was continuously purged with dry nitrogen gas to reduce terahertz absorption due to atmospheric water vapor.⁵⁻⁷ Pellets for THz-TDS measurements were prepared by grinding with PTFE to an approximate 3% w/w concentration. The mixture was then pressed under about 225 MPa of pressure in a 13-mm-diameter die (Specac), furnishing 3-mm-thick samples. Spectra were acquired at 20 K and 300 K using a custom closed cycle helium cryostat instrument (Cryo Industries, Manchester, NH, US). 20,000 time-domain waveforms were acquired and averaged, and the resultant wave-

form was Fourier transformed to produce frequency-domain terahertz power spectra. The reported absorption spectra were generated through division of the sample spectrum by that of a pure PTFE-reference. The peak positions were determined by fitting with Lorentzian functions.⁶⁻⁹

1.2 Theoretical

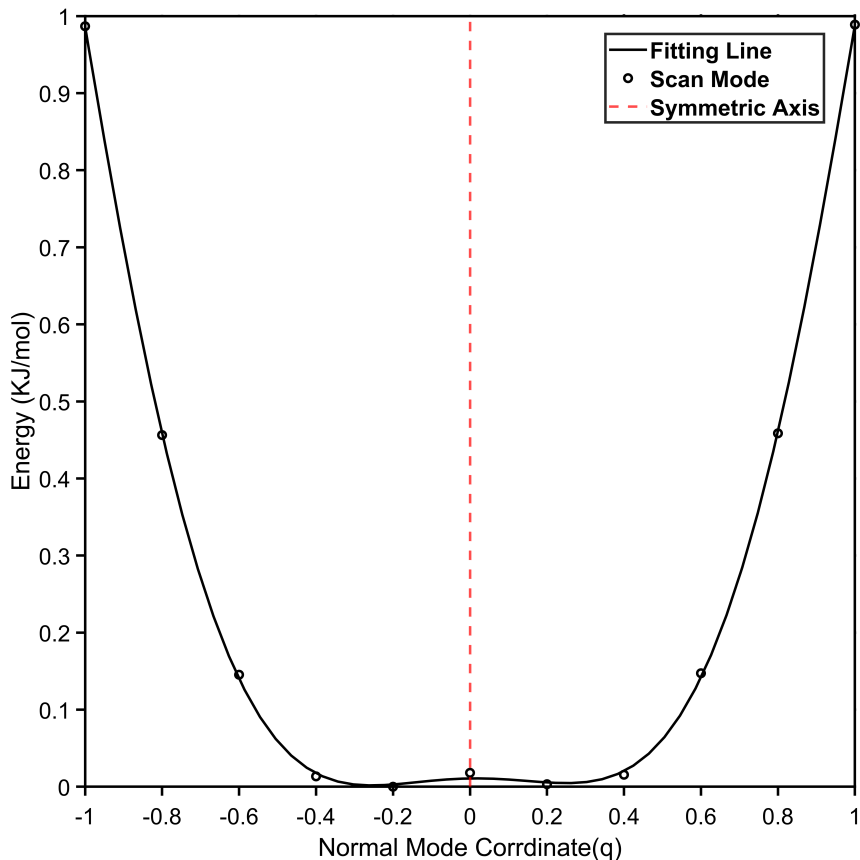
All simulations of FePO_4 were performed using the CRYSTAL17 software package,¹⁰⁻¹² which enforces three-dimensional periodic boundary conditions. The calculations employed the hybrid-GGA B3LYP functional.^{13,14} The atomic wavefunctions were represented by the Ahlrichs triple-zeta basis set with one polarization function (VTZP)¹⁵ for the iron atoms, while the non-metal atoms utilized the triple-zeta 6-311G(2d,2p) basis set.¹⁶⁻¹⁹ Reciprocal space sampling was performed using Monkhorst-Pack scheme, with 504 k-points in the irreducible Brillouin Zone for the $P1$ structures. Geometry optimizations were initiated from the experimental X-ray diffraction determined structure.²⁰ All atoms and lattice vectors were allowed to fully relax with an energy convergence criterion of $\Delta E < 10^{-8}$ hartree.¹⁰⁻¹²

Vibrational frequency calculations were executed based on the optimized structures, to yield vibrational normal modes and IR intensities. The energy convergence criterion for frequency calculations were set to a more stringent value of $\Delta E < 10^{-11}$ hartree. Eigenvalues (frequencies) and eigenvectors (normal modes) were calculated numerically through harmonic approximation.²¹ IR intensities were calculated from the dipole moment derivatives, which were determined using Berry phase method.^{10,22,23} The potential energy curves for selected normal modes were determined by displacing the structure along the chosen normal mode coordinate and calculating the energy at each step.^{12,22,24} The influence of the internal electrical field produced by the non-absorbing matrix material on the predicted terahertz spectrum was determined using PDielec package.²⁵ The particles were modeled as slab-shaped crystals, and the post-processing was performed using effective medium theory, specifically the Maxwell-Garnett mixing rule. The variable concentration in simulations were

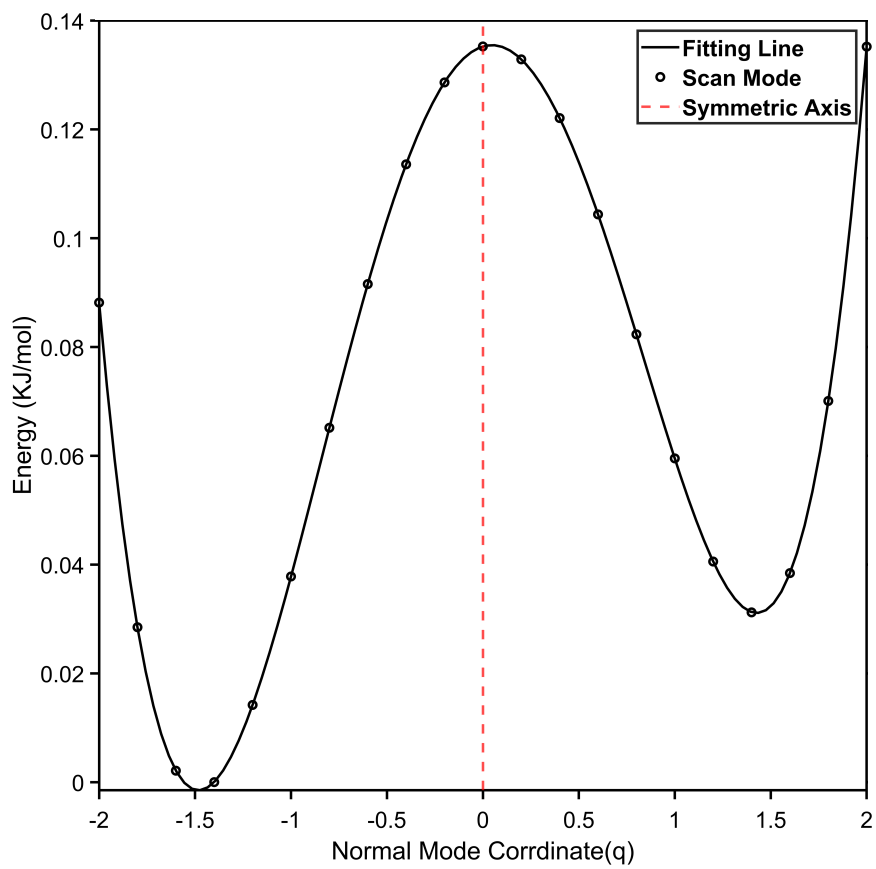
matched with experimental situation, from 10% w/w to 30% w/w, in 5% increments.

Predicted PXRD patterns were generated by the Cambridge Structural Database (CSD)-Materials package in the Mercury software. An ideal Cu K_α ($\lambda = 1.54056 \text{ \AA}$) radiation powder pattern was calculated from 5 to 50° in 2θ in step of 0.02° , with peaks convolved using a Pseudo-Voigt function.²⁶

2 Potential Energy Scans of Negative-Frequency Normal Modes



S. 1: Scan of normal coordinate for the single negative-frequency mode in the closed-shell $P3_121$ simulations, where the true minimum occurs at $q = -0.2$.



S. 2: Scan of normal coordinate for the single negative-frequency mode in the low-spin antiferromagnetic $C2$ simulations, where the true minimum occurs at $q = -1.5$.

3 Structural Parameters and Energies

Table 1: Experimental²⁰ and predicted unit cell parameters (Å), average percent deviation (%), and relative energies (kJ mol⁻¹) for the studied structures.

	Experimental	Closed Shell	HSFM	LSAFM [‡]	HSAFM
a (Å)	5.036	4.949	5.097	5.080	5.101
b (Å)	5.036	4.932	5.097	5.080	5.100
c (Å)	11.255	11.025	11.368	11.414	11.366
Avg. % Deviation	–	1.94%	1.14%	1.05%	1.18%
Rel. Energy (kJ mol ⁻¹)	–	10.459	0.029	2.733	0.0

[‡]As the structure was simulated in $P1$, in order to compare to the experimental structure this structure was generated by imposing a space group symmetry of $P3_121$ upon full-optimization.

References

- (1) Masquelier, C.; Reale, P.; Wurm, C.; Morcrette, M.; Dupont, L.; Larcher, D. Hydrated Iron Phosphates $\text{FePO}_4 \cdot n\text{H}_2\text{O}$ and $\text{Fe}_4\text{P}_2\text{O}_7 \cdot n\text{H}_2\text{O}$ as 3 V Positive Electrodes in Rechargeable Lithium Batteries. *J. Electrochem. Soc.* **2002**, *149*, A1037.
- (2) Gongyan, W. Dehydration of $\text{FePO}_4 \cdot 2\text{H}_2\text{O}$ for the Synthesis of LiFePO_4/C : Effect of Dehydration Temperature. *Int. J. Electrochem. Sci.* **2018**, 2498–2508.
- (3) Hong, Y. S.; Ryu, K. S.; Park, Y. J.; Kim, M. G.; Lee, J. M.; Chang, S. H. Amorphous FePO_4 as 3 V Cathode Material for Lithium Secondary Batteries. *J. Mater. Chem.* **2002**, *12*, 1870–1874.
- (4) Reale, P.; Scrosati, B.; Delacourt, C.; Wurm, C.; Morcrette, M.; Masquelier, C. Synthesis and Thermal Behavior of Crystalline Hydrated Iron(III) Phosphates of Interest as Positive Electrodes in Li Batteries. *Chem. Mater.* **2003**, *15*, 5051–5058.
- (5) Neu, J.; Schmuttenmaer, C. A. Tutorial: An Introduction to Terahertz Time Domain Spectroscopy (THz-TDS). *J. Appl. Phys.* **2018**, *124*, 231101.
- (6) Beard, M. C.; Turner, G. M.; Schmuttenmaer, C. A. Terahertz Spectroscopy. *J. Phys. Chem. B* **2002**, *106*, 7146–7159.
- (7) Dhillon, S. S.; Vitiello, M. S.; Linfield, E. H.; Davies, A. G.; Hoffmann, M. C.; Booske, J.; Paoloni, C.; Gensch, M.; Weightman, P.; Williams, G. P. et al. The 2017 Terahertz Science and Technology Roadmap. *J. Phys. D: Appl. Phys.* **2017**, *50*, 043001.
- (8) Jepsen, P.; Cooke, D.; Koch, M. Terahertz Spectroscopy and Imaging-Modern Techniques and Applications. *Laser Photonics Rev.* *5*, 124–166.
- (9) Burford, N. M.; El-Shenawee, M. O. Review of Terahertz Photoconductive Antenna Technology. *Opt. Eng.* **2017**, *56*, 1 – 20.

- (10) Erba, A.; Baima, J.; Bush, I.; Orlando, R.; Dovesi, R. Large-Scale Condensed Matter DFT Simulations: Performance and Capabilities of the CRYSTAL Code. *J. Chem. Theory Comput.* **2017**, *13*, 5019–5027.
- (11) Dovesi, R.; Erba, A.; Orlando, R.; Zicovich-Wilson, C. M.; Civalleri, B.; Maschio, L.; Rérat, M.; Casassa, S.; Baima, J.; Salustro, S. et al. Quantum-Mechanical Condensed Matter Simulations with CRYSTAL. *WIREs Comput Mol Sci* **2018**, *8*, e1360.
- (12) Dovesi, R.; Pascale, F.; Civalleri, B.; Doll, K.; Harrison, N. M.; Bush, I.; D’Arco, P.; Noël, Y.; Rérat, M.; Carbonnière, P. et al. The CRYSTAL code, 1976–2020 and Beyond, A Long Story. *J. Chem. Phys.* **2020**, *152*, 204111.
- (13) Ernzerhof, M.; Scuseria, G. E. Assessment of the Perdew–Burke–Ernzerhof Exchange–Correlation Functional. *J. Chem. Phys.* **1999**, *110*, 5029–5036.
- (14) Civalleri, B.; Zicovich-Wilson, C. M.; Valenzano, L.; Ugliengo, P. B3LYP Augmented with an Empirical Dispersion term (B3LYP-D*) as Applied to Molecular Crystals. *CrystEngComm* **2008**, *10*, 405–410.
- (15) Schäfer, A.; Horn, H.; Ahlrichs, R. Fully Optimized Contracted Gaussian Basis Sets for Atoms Li to Kr. *J. Chem. Phys.* **1992**, *97*, 2571–2577.
- (16) Schuchardt, K. L.; Didier, B. T.; Elsethagen, T.; Sun, L.; Gurumoorthi, V.; Chase, J.; Li, J.; Windus, T. L. Basis Set Exchange: A Community Database for Computational Sciences. *J. Chem. Inf. Model.* **2007**, *47*, 1045–1052.
- (17) Pritchard, B. P.; Altarawy, D.; Didier, B.; Gibson, T. D.; Windus, T. L. New Basis Set Exchange: An Open, Up-to-Date Resource for the Molecular Sciences Community. *J. Chem. Inf. Model.* **2019**, *59*, 4814–4820.
- (18) McLean, A. D.; Chandler, G. S. Contracted Gaussian Basis Sets for Molecular Calculations. I. Second Row Atoms, Z=11–18. *J. Chem. Phys.* **1980**, *72*, 5639–5648.

- (19) Krishnan, R.; Binkley, J. S.; Seeger, R.; Pople, J. A. Self-Consistent Molecular Orbital Methods. XX. A Basis Set for Correlated Wave Functions. *J. Chem. Phys.* **1980**, *72*, 650–654.
- (20) Ng, H. N.; Calvo, C. Refinement of the Crystal Structure of the Low-quartz Modification of Ferric Phosphate. *Can. J. Chem.* **1975**, *53*, 2064–2067.
- (21) Pascale, F.; Zicovich-Wilson, C. M.; López Gejo, F.; Civalleri, B.; Orlando, R.; Dovesi, R. The Calculation of the Vibrational Frequencies of Crystalline Compounds and Its Implementation in the CRYSTAL Code. *J. Comput. Chem.* **2004**, *25*, 888–897.
- (22) Dovesi, R.; Kirtman, B.; Maschio, L.; Maul, J.; Pascale, F.; Rérat, M. Calculation of the Infrared Intensity of Crystalline Systems. A Comparison of Three Strategies Based on Berry Phase, Wannier Function, and Coupled-Perturbed Kohn–Sham Methods. *J. Phys. Chem. C* **2019**, *123*, 8336–8346.
- (23) Cutini, M.; Civalleri, B.; Ugliengo, P. Cost-Effective Quantum Mechanical Approach for Predicting Thermodynamic and Mechanical Stability of Pure-Silica Zeolites. *ACS Omega* **2019**, *4*, 1838–1846.
- (24) Maschio, L.; Kirtman, B.; Orlando, R.; Rérat, M. Ab Initio Analytical Infrared Intensities for Periodic Systems through a Coupled Perturbed Hartree-Fock/Kohn-Sham Method. *J. Chem. Phys.* **2012**, *137*, 204113.
- (25) Kendrick, J.; Burnett, A. D. PDielec: The calculation of infrared and terahertz absorption for powdered crystals. *J. Comput. Chem* **2016**, *37*, 1491–1504.
- (26) Sacchi, P.; Lusi, M.; Cruz-Cabeza, A. J.; Nauha, E.; Bernstein, J. Same or Different – that is the Question: Identification of Crystal Forms from Crystal Structure Data. *CrystEngComm* **2020**,